# High angular resolution K-band spectroscopy of the nucleus of NGC 1068 with PUEO-GRIF (CFHT)

Damien Gratadour, Yann Clénet, Daniel Rouan, Olivier Lai, Thierry Forveille

A&A 411, 335–342 (2003)
DOI: 10.1051/0004-6361:20031376


Astronomy & Astrophysics

# High angular resolution *K*-band spectroscopy of the nucleus of NGC 1068 with PUEO-GRIF (CFHT)

D. Gratadour[1], Y. Clénet[1], D. Rouan[1], O. Lai[2], and T. Forveille[2]

[1] LESIA, Observatoire de Paris, 5 place Jules Janssen, 92195 Meudon, France
e-mail: firstname.lastname@obspm.fr
[2] CFHT Corporation, 68-1238 Mamalahoa Highway, Kamulea HI 96743, USA

Received 21 January 2003 / Accepted 7 July 2003

**Abstract.** We provide new high angular resolution *K*-band spectroscopic observations of the nucleus of NGC 1068 obtained with the new 3-D spectrograph GriF coupled to PUEO, the CFHT adaptive optics system. Results match well with the general framework of the unified model of active galactic nuclei (AGN) and bring more precise evaluation of the size and structure of the close AGN environment. The *K*-band emission is dominated by the thermal continuum of the compact central source (albeit resolved: $FWHM \sim 0.12''$) with a color temperature around 950 K (reddened sublimation temperature of the dust, corresponding to 1200 K when deredenned), interpreted as the border of a sublimation cavity within the dust torus, surrounding the central core. Coronal emission lines ([Si VI], [Si VII] and [Ca VIII]) are detected from a few tenths of arcseconds around this compact source and a new [Si VI] emission spot is found at 0.7″ north of the central source. The Brackett $\gamma$ emission features a very broad component ($FWHM = 2500$ km s$^{-1}$) in the central 200 mas and we claim that it correponds to the broad line region seen through the dust. A narrower component ($FWHM = 1600$ km s$^{-1}$) is seen at larger angular distance and is likely the trace of the narrow line region. Molecular hydrogen emission lines are detected beyond 0.6″ of the central source. We interpret the lack of emission in the center as a lack of excited molecular $H_2$ along the line of sight, because of the putitative dust torus shading gas from UV photons. No evidence of stellar activity in a 1″ radius around the central source can be found. We also compare these observations to the results of a numerical model of a torus harboring an active galactic nucleus. The main characteristics of the observed spectra (slope, flux) match well with the unified scheme of AGN, in the case of a dense ($\tau_V = 40$) obscuring torus containing silicate grains with an inclination angle of around 22° with regards to the line of sight.

**Key words.** galaxies: Seyfert – galaxies: individual: NGC 1068 – infrared: galaxies – instrumentation: adaptive optics – instrumentation: spectrographs – radiative transfer

## 1. Introduction

High angular resolution with adaptive optics (AO) in the near infrared is an ideal tool to probe galactic nuclei close environment and to test the unified scheme of active galactic nuclei (AGN). This model (Krolik 1990; Granato & Danese 1993) assumes that the compact nucleus (a massive black hole with an accretion disk) is surrounded by a dusty molecular torus whose direction with regards to the line of sight is responsible for the main differences between Seyfert I and Seyfert II nuclei. Infrared observations are obviously powerful since the best AO performances are obtained in this wavelength range and the dust of the tori, which is assumed to hide the activity of Seyfert II nuclei, is more transparent in the IR, allowing spectral studies and imaging of the inner parts of type II nuclei.

Antonnucci & Miller (1985) laid the foundation for this unified scheme with their observations of broad permitted lines in polarized light in NGC 1068, the archetypal Seyfert II nucleus, inferring the presence of a hidden Seyfert I nucleus. Several hints have since reinforced the plausibility of this scheme: radio observations of a compact ionized disk (Gallimore et al. 1996a) and detection of an extended CO disk (Schinnerer et al. 2000). Rouan et al. (1998) may have obtained the first images of the torus of NGC 1068 in the near-IR, and some authors have strengthened this interpretation through AO imaging (Marco & Alloin 2000) and spectroscopic studies with large telescopes (Alloin et al. 2001; Galliano & Alloin 2002), yet without AO.

Located at an approximate distance of 15 Mpc (1″ ∼ 70 pc), NGC 1068 is one of closest, brightest and most studied Seyfert nucleus. In this paper, we report on near-infrared long-slit spectroscopic observations of the core of this Seyfert nucleus made with GriF, the new 3-D spectrograph coupled with PUEO, the CFHT adaptive optics system. First, in Sect. 2, we give a short description of the observing conditions and data processing. Section 3 is dedicated to the extraction of physical and morphological parameters from the shape of the continuum and the characteristics of emission lines. These results

*Send offprint requests to*: D. Gratadour,
e-mail: damien.gratadour@obspm.fr

are compared in Sect. 4 to the output from a radiative transfer model and we discuss how well they match predictions from the unified model. We conclude in the last section.

## 2. Observations

### 2.1. Data acquisition

Long slit spectra of the nucleus of NGC 1068 were obtained during a technical run of GriF (Clénet et al. 2002), a 3-D spectrograph coupled with the CFHT adaptive optics system PUEO (Rigaut et al. 1998). GriF was used in its long slit mode with a 0.3″ slit. Data were collected with the KIR camera whose pixel scale is 0.0348″.

The AO system was servoed on the nucleus of the galaxy itself, leading to a spatial resolution of 0.12″. The efficiency of the AO correction for this kind of extended reference source with PUEO has already been discussed in Rouan et al. (1998). The spectral resolution of the GriF long slit mode is about 230, measured from the *FWHM* of lines produced by an argon calibration lamp.

Six long slit spectra of NGC 1068 were obtained with a 300 s integration time for each. The slit axis was along PA = 5°. In order to obtain a spectrum of the atmospheric transmission and a 1-D PSF, long slit spectra of HD 40335, an A0IV reference star, were also acquired.

### 2.2. Data reduction

We have first applied bad pixel and flat field corrections. The misalignment of the grism with regard to the plane of the camera and the slit induces respectively a rotation of spectra with respect to the axis of the detector and a quasi-linear shift of each spectrum with regard to its neighbors. The inverse transformations, rotation and shift, have been applied to remedy these effects. Then, three individual line spectra were averaged to match the spatial resolution of the observations.

Atmospheric corrections are required since the *K*-band is severely affected by atmospheric emission and absorption. In order to correct spectra for atmospheric emission, sky spectra were built for each individual image by computing a median spectrum along the slit. A composite spectrum of the atmospheric transmission was also built by combining the obtained spectrum of HD 40335 with a theoretical spectrum of an A0 IV star (Pickles 1998). The sky spectrum was subtracted from each raw spectrum and the obtained spectra was corrected with the composite spectrum of the atmospheric transmission. The final spectra for several positions along the slit are displayed in Fig. 1.

## 3. Results

### 3.1. Continuum source

The maximum emission spectrum is, as expected, totally featureless at the level of uncertainty reached after processing (features appearing in Fig. 1 in the maximum spectrum are interpreted as unperfectly corrected atmospheric features). We assume, as commonly accepted (see Thatte et al. 1997 for a more detailed discussion), that this maximum emission spectrum is centered on the true nucleus of NGC 1068 which corresponds to the radio source S1 detected by Gallimore et al. (1996b). All spectra, north and south of this central spectrum within a distance of 1″ are more or less dominated by a similar quasi-power law continuum. Since this near-IR continuum is not polarized in most Seyfert II nuclei, it can hardly be reflected light and is generally interpreted as dust emission arising near the central engine.

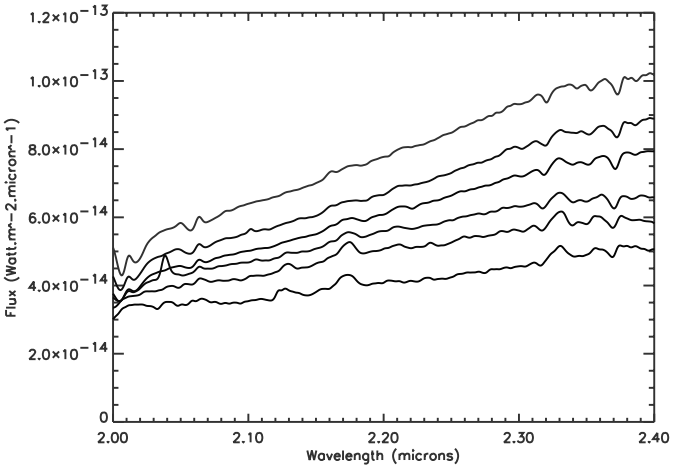


**Fig. 1.** Spectra at several locations along the slit. Up to down: maximum emission, +0.1″, +0.3″, +0.5″, +0.7″ and +1.0″ north. Spectra around the maximum spectrum have been re-scaled so that the units of flux are representative only for the maximum spectrum.

**Table 1.** Values of the power-law spectral index for different positions along the slit around the spectrum of maximum emission.

| Position | $\beta$ | Position | $\beta$ |
|---|---|---|---|
| max | 2.9 | | |
| +0.1″ north | 2.9 | +0.1″ south | 2.4 |
| +0.2″ north | 1.9 | +0.2″ south | 1.7 |
| +0.3″ north | 2.9 | +0.3″ south | 2.4 |
| +0.4″ north | 2.1 | +0.4″ south | 1.9 |
| +0.5″ north | 2.2 | +0.5″ south | 1.7 |
| +0.6″ north | 1.5 | +0.6″ south | 1.6 |

#### 3.1.1. Dust temperature

Firstly the slope of the *K*-band continuum can be examined to determine whether it corresponds to thermal or non-thermal emission. For that purpose, spectra are smoothed by a convolution with a broad (20 pixel) Gaussian distribution to remove emission and absorbtion features and to improve the S/N ratio. A power law, $F_\gamma \propto \lambda\, F_\lambda \propto \lambda^{\beta+1}$, is then fitted to the smoothed spectra.

Results, compiled in Table 1, are consistent with the conclusions of Thatte et al. (1997) and references therein. They unambiguously indicate a thermal emission since the spectral index is much steeper than expected in the non-thermal case.

**Table 2.** Values of the parameters of the fitted Black Body distribution at different locations along the slit.

| Position | Temperature | $\alpha$ |
|---|---|---|
| +0.3″ north | 927 | 1.71 |
| +0.2″ north | 971 | 1.96 |
| +0.1″ north | 961 | 1.56 |
| max | 935 | 1.52 |
| +0.1″ south | 948 | 1.55 |
| +0.2″ south | 948 | 2.04 |
| +0.3″ south | 893 | 2.27 |

If the continuum emission at these wavelengths is interpreted as reddened thermal black body emission from the hot dust surrounding the active nucleus, one can fit a Black Body distribution, weighted by a power law emissivity, on the smoothed spectra:

$$F_\gamma \propto \lambda B_\lambda \lambda^{-\alpha} \quad \text{with} \quad B_\lambda = \frac{2\,hc^2}{\lambda^5} \exp\left(\frac{-hc}{\lambda kT}\right).$$

Table 2 gives the values of the two parameters ($T$, the temperature and $\alpha$, the index of the dust emissivity law) of the fitted Black Body distribution at different locations along the slit around the maximum emission.

The adjusted mean temperature of these inner parts of the nucleus is about 950 K. This is a lower limit of the actual dust temperature: in fact, it corresponds to the reddened emission of hotter dust seen through a dusty absorbing environment. This dust, very close to the nucleus, must be heated by the strong UV radiation field and some evidence (see references in Thatte et al. 1997) seems to indicate that it is near the sublimation temperature. This is expected if we assume that it corresponds to the inner wall of the cavity around the central engine. Note, however, that some authors disagree with this simplistic interpretation (Pier & Krolik 1993), proposing that outgasing of warm dust below the sublimation temperature should be taken into account. In any case, very hot dust is mandatory to explain the observed slope. This sublimation temperature and the slope of the *K*-band continuum depend on the nature of the dust grains (silicates, graphites, ...). A more detailed study relying on a radiative transfer model is proposed in the next section.

An evolution of the dust temperature along the slit can be noticed. Hotter dust seems to appear symmetrically at 0.2″ north and south of the maximum emission (Table 2). These locations correspond to a break in the slope of the *K*-band continuum listed in Table 1. This might be the signature of an other type of radiation source (young stars rather than dust heated by the central core), or more likely due to a reduced opacity when getting out from the torus, which makes the hot dust emission bluer.

### 3.1.2. Size of the central continuum source

In order to measure the size of the central continuum source and to get a better understanding of the rupture in the evolution of the slope, we have deconvolved the light profile of NGC 1068 with the profile of the reference star. We used the maximum likelihood deconvolution algorithm found in the IDL astro library. The main result of the deconvolution process is the resolution of the compact central continuum source, with a *FWHM* of 0.12″. This is around the diffraction limited resolution of the instrument, but appears significant. It allows us to put a maximum value of 0.12″–0.15″ on the north-south extension of the source and excludes a size as large as 0.2″.

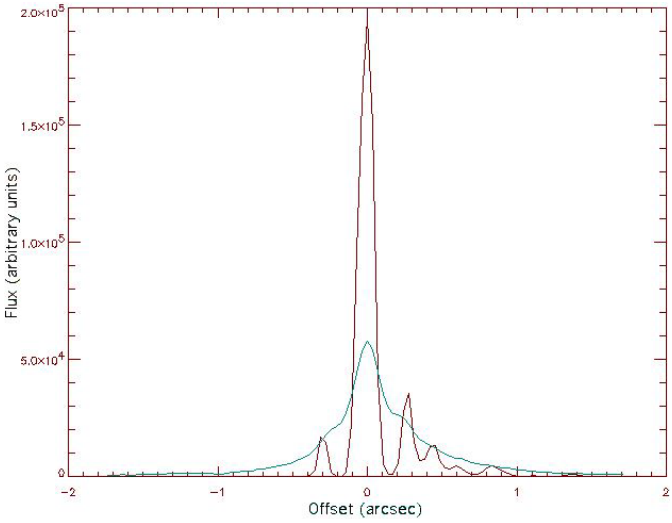


**Fig. 2.** Deconvolved light profile (black) of NGC 1068. The undeconvolved profile is plotted in grey.

Two secondary sources appear symmetrically at +0.3″ north and south of the primary source on the deconvolved profile (Fig. 2). These sources could be linked to the evolution of the slope of the continuum and temperature around the central engine. Unfortunately, as the performances of the AO system, and so the shape of the PSF, depends on the nature (extended or pointlike) and magnitude of the sources, we cannot put a strong weight on this result. The two secondary sources could then be artefacts of the deconvolution process.

## 3.2. Emission lines

Emission lines (coronal as well as low ionization ones) are the best AGN tracers. Indeed, the main difference between Seyfert I and Seyfert II nuclei is the presence or not of a directly observable broad line region (BLR), while a narrow line region (NLR) is detectable in both types of active nuclei. The fact that the BLR seems to appear in polarized light in some Seyfert II nuclei (Antonnucci & Miller 1985; Miller et al. 1991) is one of the corner-stones of the unified model.

### 3.2.1. H Brackett $\gamma$

The Brackett $\gamma$ emission line is supposed to emerge from the BLR as well as from the NLR. Many authors had detected this line with a narrow width in the nucleus of NGC 1068 (Oliva & Moorwood 1998; Tamura et al. 1991; Thomson 1996) with lower angular resolution long-slit spectroscopic observations.

In our spectra, a blueshifted (about 1500 km s$^{-1}$) broad component (*FWHM* about 2500 km s$^{-1}$) seems to appear very close to the maximum emission spectrum (respectively +0.1″ and 0.2″ north and south), hence likely tracing the BLR seen through the dust. Because of the residual effect of the (non-redshifted) unperfectly corrected Brackett $\gamma$ line in the spectrum of the calibration star used for atmospheric absorption correction, we cannot put a strong weight on this claim. However, we note the coherence of the width of these lines, with typical widths of polarized broad lines seen by Antonnucci & Miller (1985); Miller et al. (1991).

This must be considered as a rough estimate, as the accuracy of the fit realized over this weak component is not fully satisfactory. We will see in the next section how this value is consistent with our best model of an obscuring torus. This possible detection of the BLR might be linked to the work of Goodrich et al. (1993) who found an obscured broad Pashen $\beta$ line in three Seyfert II nuclei.

Our spectra reveal also a narrow component beyond 0.1″ north and south of the maximum emission spectrum, whose intensity decreases with distance to the maximum. This narrow component is blended with the broad one at 0.2″. The width of the narrow component is $FWHM = 1650(\pm 300)$ km s$^{-1}$ which is consistent with values expected for lines emerging from the NLR. The intensity of the south narrow component is lower than the north one beyond 0.2″ implying more obscuration by material on the line of sight, probably because of the inclination of the torus axis on the plane of the sky, a well established result (Packham et al. 1997). The fact that the NLR appears only beyond 0.1″ north and south is consistent with the expected location of this region and size of the obscuring torus (0.1″ $\sim$ 7 pc). The evolution of the line intensity is plotted in Fig. 3. The lower intensity of the south component is an indication of an inclination of this torus. In this simple scheme, the Brackett $\gamma$ lines seen on spectra of regions located at 0.2″ north and south of the maximum emission spectra must emerge from the vicinity of the torus.

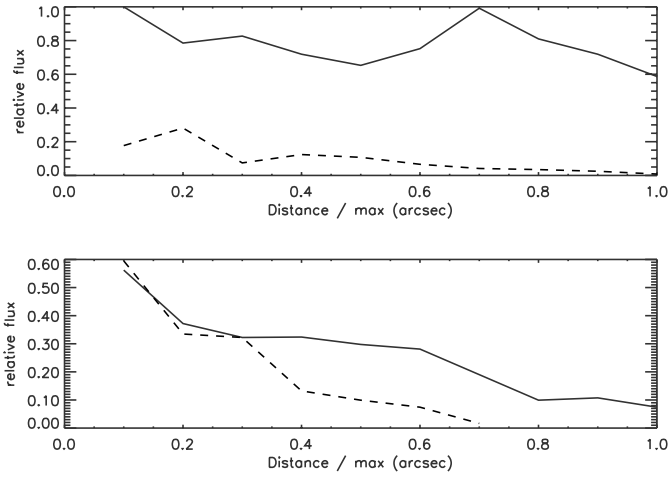


**Fig. 3.** The [Si VI] (top figure, solid line: north, dashed line: south) and Bracket $\gamma$ (solid line: north, dashed line: south) line intensity evolution along the slit. Distance to the maximum is in arcsec and flux is relative to the 0.1″ line flux. In the Brackett $\gamma$ case, only the narrow component is plotted so the 0.1″ line flux is not unity.

### 3.2.2. Coronal lines

Coronal lines are forbidden high ionization lines associated with the NLR. The structure of this region is very complex and these lines testify to specific mechanisms able to "peel" atoms almost totally (ionization by hard UV or collision in a very hot medium). An ionization cone has been detected in visible and UV in NGC 1068 (Unger et al. 1992 especially through low ionization lines) whose direction is correlated to the direction of the jet, with a wider aperture angle. Moreover, the very high excitation ionization lines were found to follow the conical morphology of lower ones as seen in X-rays by Ogle et al. (2003).

The coronal line region (CLR) can be considered apart since atoms are nearly totally ionized. As the width of these lines is narrow, the CLR is always associated with the NLR, but the very high ionization degree suggests a particular excitation mechanism and location (Murayama & Taniguchi 1998), with maybe maser emission (Greenhouse et al. 1993). A broad band (IR to visible) survey of coronal lines in NGC 1068 is proposed in Marconi et al. (1994). Among these features, we detect the [Si VI], [Si VII] and [Ca VIII] lines.

The [Si VI] ($\lambda = 1.962$ $\mu$m, $E_{\rm ion} = 205$ eV) line has been detected in many Seyfert galaxies (Marconi et al. 1994) and is considered as a tracer of the Seyfert activity. The very high transition rate (2.38 s$^{-1}$) induces very powerful lines all along the slit, compared with the other coronal lines. This line seems to be blended with either a molecular hydrogen line ($v = 1{-}0$ S3) or a residual atmospheric feature which distorts it, and so the measured width and integrated flux are not so accurate. The first hypothesis can be eliminated because this would be the only $H_2$ S3 line to be detected which is very unlikely as several lines corresponding to lower rotational levels are not detected (see next subsection).

In our spectra, the [Si VI] emission appears from 0.1″ north and south of the maximum emission spectrum. The south component seems to be highly attenuated since the intensity of the north component is five to ten times greater. The *FWHM* of these lines is around 1650 km s$^{-1}$ ($\pm$400 km s$^{-1}$), and the intensity of the two components (north and south) decreases with the distance to the maximum spectrum. There is an emission peak at +0.7″ north which could correspond to the radio peak found in Gallimore et al. (1996b) at 0.5″ north of the radio source S1 interpreted as an interaction of the jet with NLR clouds. A more precise absolute astrometric measurement would be necessary to ascertain this hypothesis. A similar correlation with radio maps has been made in Thompson et al. (2001) with a [Si VI] peak at 1.6″ north in a mapping at a larger scale.

We also detect the [Si VII] emission line at 2.483 $\mu$m, but given the fact that its wavelength is near the edge of the transmission wavevelength domain of the filter and in a part of the *K*-band very affected by atmospheric effects, we only claim the detection of this line without any measurement of width or flux.

On the same line, we assert that the [Ca VIII] emission line at 2.321 $\mu$m is also detected in some of the north spectra but

**Table 3.** Values of the molecular hydrogen line ratios and temperatures found at different locations along the slit.

| Position | $\frac{(v=1-0)S2}{(v=1-0)S0}$ | $\frac{(v=2-1)S1}{(v=1-0)S0}$ | Temperature |
|---|---|---|---|
| <0.8″ north | ∼0.5 | - | ∼500 K |
| +0.8″ north | ∼1. | 0.3 | ∼1000 K |
| >0.8″ north | <0.5 | <0.3 | <500 K? |

the measurements of its width and flux are also affected by atmospheric effects partially corrected.

A wider band spectroscopic study (including visible and all near-IR bands) is necessary to improve models on the physical conditions in the CLR since lines ratios are obviously unavoidable to derive more physical information.

#### 3.2.3. Molecular hydrogen

The ($v1-0$)S1 and ($v1-0$)S0 molecular hydrogen lines have already been detected in the nucleus of NGC 1068 (Oliva & Moorwood 1998; Moorwood & Oliva 1990; Thomson 1996; Alloin et al. 2001). The results of Moorwood & Oliva (1990) are consistent with a thermal excitation mechanism. Maps of the ($v1-0$)S1 emission in different apertures around the core have also been made. The main conclusions are: firstly, the distribution of $H_2$ emssion region in several knots and the possible connexion between molecular hydrogen emission knots and the shape of the border of the radio jet emission on large scale (Blietz et al. 1994, with a $5'' \times 5''$ map); and secondly an estimation of the core mass which is about $10^8$ solar mass (Alloin et al. 2001), within a 70 pc radius around the central engine, from the velocity difference of these knots.

In our spectra, several $H_2$ lines are detected, but, and this is probably the most important result of our observations of $H_2$, there is a lack of molecular hydrogen emission in the direct vicinity of the nucleus, previously observed by Galliano & Alloin (2002) with a lower (seeing limited) angular resolution. The ($v1-0$)S1 line appears symmetrically beyond 0.4″ north and south, and the ($v1-0$)S0 and ($v1-0$)S2 appear beyond 0.6″ north. Contrary to the Brackett $\gamma$ emission evolution, the intensity of the molecular hydrogen lines increases with distance to the maximum emission and does not have a quasi-linear evolution. The width of those lines is about the spectral resolution of the instrument ($FWHM \sim 1200$ km s$^{-1}$). The S1(1−0)/S0(1−0) line ratio is around 3.3 and the S1(2−1)/S0(1−0) ratio is lower than 0.1 since the S1(2−1) line is not clearly detectable. Such ratios are consistent with thermal excitation mechanisms (Black & Van Dishoeck 1987), at an excitation temperature lower than 2000 K.

In order to estimate an excitation temperature and the nature of the thermal mechanism, the S2(1−0)/S0(1−0) ratio was plotted versus the S1(2−1)/S1(1−0) ratio (Mouri 1993). Indeed, the location of the observed point in this diagram is a function of the excitation mechanism and of the kinetic temperature when collisions dominate. The S2(1−0)/S0(1−0) ratio we measured spans a large range, so

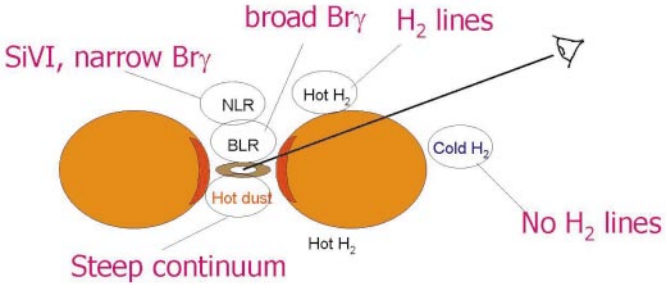


**Fig. 4.** Simple model synthetising the morphological properties of the object consistent with our observations.

temperatures are found between 500 and 1000 K. On the other hand, the S1(1−0)/S0(1−0) ratio is consistent with photodissociation but this mechanism should induces homogenous evolution of the temperature when going away from the excitation source.

These results appear to be globally consistent with thermal excitation by UV in a complex environment with obscuring material between the excitation source and the $H_2$ gas. The latter begins to become a source of emission lines only when UV photons are able to reach it, i.e. at a distance of the line of sight beyond the border of the torus, as depicted in Fig. 4, the excitation temperature is then equal to or lower than 1000 K.

### *3.3. Stellar component*

Looking for traces of a stellar component is important since:

- Young star activity, detectable through H and He absorption features or through CO lines tracing giant and supergiants, is also invoked to power active nuclei in alternative models (Terlevich et al. 1987, 1995).
- Boisson et al. (2000) claimed that the stellar population and activity may depend on AGN type, a correlation that would not be explained by the standard unified model. However, the difficulty of selecting a homogeneous sample of both Seyfert 1 and 2 nuclei may introduce a bias in their study.

A composite continuum (power law fitted on the highly smoothed spectra) has been subtracted from each of our spectra to make CO band heads and He and H absorbtion features conspicuous. No stellar activity is clearly detectable in the central 1″ around the nucleus in our spectra, but the strength of the continuum might totally hide these absorbtion features. This is not enough to exclude a stellar component in the activity of the inner parts of the nucleus and many authors (especially Thatte et al. 1997) have argued that stellar activity is a non-negligible fraction of the luminosity of the nucleus at other wavelengths.

## 4. Radiative transfer model and discussion

### *4.1. Description of the model*

We have built a radiative transfer code similar to those previously developed by different authors (Granato & Danese 1993; Granato et al. 1996). We assume a compact central continuum (UV and visible) source, which illuminates its neighborhood

isotropically, and whose luminosity is $1.5 \times 10^{45}$ ergs s$^{-1}$, according to the measured bolometric luminosity, as in Granato & Danese (1993). The nature and physical state of the medium surrounding the central source depends on temperature. As long as the temperature is higher than the sublimation temperature of the dust ($T_{\rm sublim} = 1400$ K in the case of silicate grains), radiation propagates in a transparent cavity. The radius of this cavity ($r_{\rm in} \approx 5\,L_{46}^{1/2}$ where $L_{46}$ is the luminosity of the primary visible-UV source in units of $10^{46}$ ergs s$^{-1}$) is considered as the inner radius of the dusty molecular torus. The density distribution beyond this radius is described by $e^{-k\cos^2\theta}$ with $k = 6$ according to Granato & Danese (1993).

The radiative transfer equation is:

$$\nabla\, I_\nu = -\alpha_\nu\, I_\nu + j_\nu$$

where $I_\nu$ is the specific intensity, and $\alpha_\nu$ and $j_\nu$ are respectively the extinction and emission coefficients. $I_\nu$ can be split into two terms: $I_{1\nu}$ and $I_{2\nu}$ where the first component is the contribution of the central source and $I_{2\nu}$ of the dust emitted or scattered emission.

The mean specific intensity reads then $J_\nu = J_{1\nu} + J_{2\nu}$ with:

$$J_{1\nu 1} = \int I_{1\nu} {\rm d}\Omega = \frac{1}{4\pi}\frac{L_\nu^c(\theta)}{4\pi r^2}\exp^{-\tau_\nu(r,\theta)}$$

where $\tau_\nu(r,\theta)$ is the optical depth, $L_\nu^c(\theta)$ the primary luminosity. The second component is the radiation emitted or scattered by the dust:

$$J_{2\nu} = \int L_{\nu,\rm grains} 4\pi a^2 \rho_{\rm grain}(r,z)\exp^{-\tau_\nu(r,\theta)}\frac{{\rm d}r}{\cos(\theta)}{\rm d}\Omega$$

$$L_{\nu,\rm grains} = Q_{{\rm a}\nu} B_\nu(T) + Q_{{\rm s}\nu} J_\nu$$

where dust grains are considered as grey bodies of radius $a$, density $\rho_{\rm grain}(r,z)$, and respectively scattering and absorbtion efficiencies $Q_{\rm a}$ and $Q_{\rm s}$. Temperature is derived by solving numerically the radiative equilibrium equation

$$\int_0^\infty Q_{{\rm a}\nu} J_\nu\, {\rm d}\nu = \int_0^\infty Q_{{\rm a}\nu} B_\nu(T)\, {\rm d}\nu.$$

An iterative scheme is used that converges within three or five steps. A visualization code builds an intensity map at different wavelengths and SED of the object. The main parameters of the model are the size, the inclination angle of the torus with regards to the line of sight and the dust properties (composition: silicate or graphite grains, optical depth).

### 4.2. Results

The slope and intensity of the *K*-band continuum are best reproduced with silicate grains, an optical depth in the equatorial plane of $\tau_V = 40$ in the visible wavelengths range, and an inclination angle of 22° of the torus with regards to the line of sight. This leads to an extinction of $\tau_V = 13.7$ ($\tau_K = 1.25$ only in the *K*-band) in the direction of the line of sight. The slope of continuum emission obtained with graphite grains are by far too steep (Fig. 5). This might be due to the higher sublimation temperature of the graphites (1750 K compared to 1400 K for silicates). Another critical parameter is the inclination angle whose range is as narrow as ±2° in order to obtain a good fit both in term of absolute flux and slope.

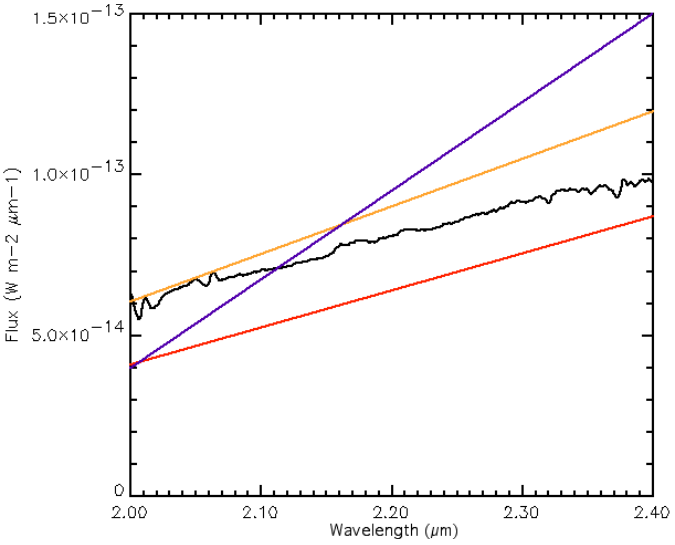


**Fig. 5.** Spectra obtained with the model plotted over the observed spectrum (black) in a 0.2″ apperture around the maximum. Yellow and red spectra were obtained with a torus of optical depth $\tau_V = 40$, silicates grains and an inclination angle of respectively 25 and 20° with regards to the line of sight. The blue spectrum is obtained with graphite grains, $\tau_V = 200$ and 22°.

These results are consistent with conclusions made by Thatte et al. (1997) who obtained a temperature of 1440 K in the case of optically thick dust emission, and represent a direct confrontation between observations and the unified scheme. At 2.2 microns, the images obtained with the visualization code are dominated by a central source whose *FWHM* is around 0.1″ and whose location corresponds to the location of the compact central source: this matches very well with observations. The 950 K central temperature found in the study of the continuum (see Sect. 3) might be a reddened temperature of this *sublimation caity* of dust surrounding the central core, seen through the dusty torus. The hot wall of the cavity is then identified with the quasi-pointlike source observed in the *K*-band. As the wavelength increases, the quasi-pointlike source is sliding north and its width is increasing, as clearly visible in Fig. 6.

The other point to focus on is the broad Bracket $\gamma$ component flux estimated previously. Thanks to the comparison of the observed continuum slope and intensity against the model, we find an extinction along the line of sight of $\tau_K = 1.25$ in the *K*-band. This leads to a primary (i.e. if unobscured by the torus) broad Brackett $\gamma$ luminosity of $L_{{\rm Br}\gamma} = 1.35 \times 10^{-16}$ W m$^{-2}$, in a 0.3″ × 0.3″ aperture around the core, and so $L_{{\rm Br}\gamma} = 3.2 \times 10^{-3} L_{K_{\rm tot}}$ where $L_{K_{\rm tot}}$ is the total *K*-band luminosity in this aperture. This value would lead to an intrinsic Brackett $\alpha$ luminosity of 3.1 $L_{{\rm Br}\gamma}$ and thus to a predicted observable luminosity of $2.4 \times 10^{-16}$ W m$^{-2}$, using $\tau_K = 1.25$ and $A_{{\rm Br}\alpha}/A_v = 0.051$ Lutz et al. (1997). This value is consistent with the upper limit ($8 \times 10^{-16}$ W m$^{-2}$) deduced by Lutz et al. (2000) for the broad component.

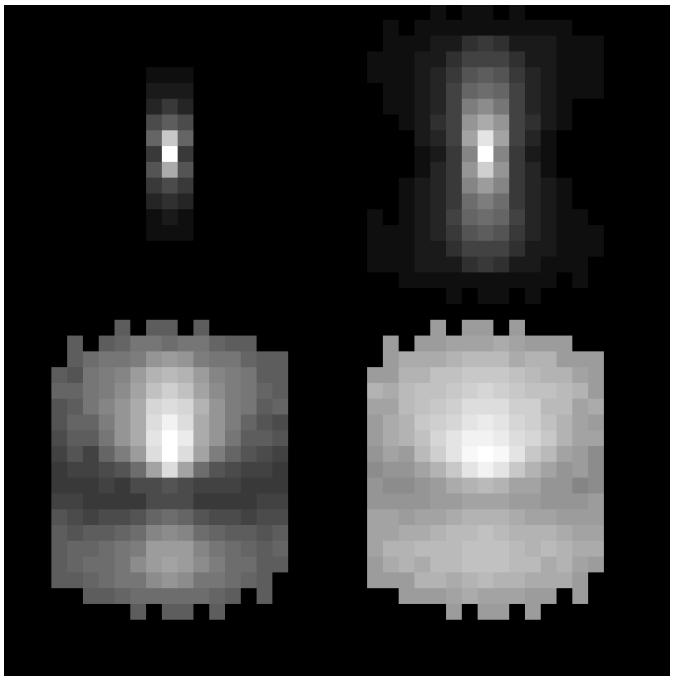

**Fig. 6.** Images at (from up-right and clockwise) 2.2, 5, 10 and 20 $\mu$m obtained with the radiative transfer model. Pixel scale: 0.06″. Power law scale representation (index = 0.1).

The extinction of $A_v = 14$ on the line of sight is much lower than the value proposed by Pier & Krolik (1993) in their compact torus model. It is closer to the one used by Granato et al. (1996) even if significantly smaller. However, this value is consistent with the lower limits of Lutz et al. (2000) in their study of possibly broad Pfund $\alpha$ emission, where they find the lowest limit of their study. For other lines (Brackett $\beta$ and Brackett $\alpha$), their minimum value is higher and so not consistent with our study. However, this value might depend on the considered inclination of the obscuring material.

All these clues are clearly in favor of a moderately thick extended torus model.

## 5. Conclusion

These first high angular resolution *K*-band spectroscopic observations of the nucleus of NGC 1068 match well with the general framework of the unified model of AGN.

The main results supporting this conclusion are the following:

- The hot dust emission seems to be confined in a quasi-resolved region of 0.1″–0.15″ (∼7–10 pc) radius around the core: this is the expected size of the sublimation cavity of dust for the estimated luminosity of the AGN.
- The slope of the continuum indicates a color temperature of 950 K, which corresponds to a reddened temperature of hotter dust (1400 K in the case of silicates).
- There is a jump in the observed color temperature at 0.2″ from the center both north and south: it may be due to a sudden drop in reddening, as expected if the line of sight no longer crosses the obscuring torus at these locations.
- Molecular hydrogen emission lines are detected only at a distance larger than 30 pc of the central source, which is consistent with a toroidal shape of obscuring material: no excited $H_2$ can be found on lines of sight crossing the thickest part of the torus because UV radiation cannot reach it. In the outermost part where several ortho and para $H_2$ lines are detected, the line ratios are consistent with thermal ionization mechanisms, like collisions, and an excitation temperature around 1000 K.
- Tracers of the NLR ([Si VI] and Brackett $\gamma$ emission line) are also detected from the first few 0.1″ around the core. An emission spot of [Si VI] is also detected at 0.7″ north of the central source.
- The comparison of the observed *K*-band continuum with a numerical model leads us to fix the optical depth ($\tau_V = 40$ in the equatorial plane), composition (silicates), and inclination of the torus with regard to the line of sight (∼22°).
- A broad Brackett $\gamma$ emission line seems to appear but its weakness and the residual atmospheric effects forbid any precise measurement. Nevertheless, the approximate measurement of its intensity in a $0.2'' \times 0.3''$ aperture and the extinction parameters found with the numerical model are consistent with constraints fixed in previous studies.

It seems that a wider band spectroscopic and imaging study (including optical and the other near-IR bands) with high angular resolution, as achievable with the new NAOS-CONICA system (VLT), will lead to a better understanding of the morphology of the closest AGN core, and particularly the exact dimensions of the torus and the mechanisms involved in its interaction with its neighborhood. These first observations obtained with the new GriF spectrograph coupled to PUEO strengthen the efficiency of adaptive optics in the study of the AGN phenomena.

## References

Alloin, D., Galliano, E., Cuby, J. G., et al. 2001, A&A, 369, L33
Antonnucci, R. R. J., & Miller, J. S. 1985, ApJ, 267, 621
Boisson, C., Joly, M., Moultaka, J., et al. 2000, A&A, 357, 850
Black, J. H., & Van Dishoeck, E. F. 1987, ApJ, 322, 412
Blietz, M., Cameron, M., Drapatz, S., et al. 1994, ApJ, 421, 92
Clénet, Y., le Coärer, E., Joncas, et al. 2002, PASP, 114, 563
Galliano, E., & Alloin, D. 2002, A&A, 393, 43
Gallimore, J. F., Baum, S. A., O'Dea, C. P., et al. 1996a, ApJ, 462,740
Gallimore, J. F., Brown, S. A., & O'Dea, C. P. 1996b, ApJ, 464, 198
Goodrich, R. W., Veilleux, S., & Hill, G. J. 1993, ApJ, 422, 521
Granato, G. L., & Danese, L. 1993, MNRAS, 268, 235
Granato, G. L., Danese, L., & Franceschini, A. 1997, ApJ, 486, 147
Greenhouse, M. A., Feldman, U., Smith, H. A., et al. 1993, ApJS, 88, 23
Krolik, J. H. 1990, Active Galactic Nuclei (Princeton: Princeton University Press)
Lutz, D., et al. 1997, in First ISO workshop on analytical spectroscopy, ed. A.M. Heras et al., ESA SP-419 (Noordwijk: ESA), 143
Lutz, D., Genzel, R., Sturm, E., et al. 2000, ApJ, 530, 733
Marco, O., & Alloin, D. 2000, A&A, 353, 465
Marconi, A., Van der Werf, P. P., Moorwood, A. F. M., et al. 1996, A&A, 315, 335

Marconi, A., Moorwood, A. F. M., Salvati, M., & Oliva, E. 1994, A&A, 291, 18
Miller, J. S., Goodrich, R. W., & Matthews, W. G. 1991, ApJ, 378, 47
Moorwood, A. F. M., & Oliva, E. 1990, MNRAS, 300, 388
Mouri, H. 1993, ApJ, 427, 777
Murayama, T., & Taniguchi, Y. 1998, ApJ, 497, L9
Oliva, E., & Moorwood, A. F. M. 1998, MNRAS, 300, 388
Ogle, P. M., Brookings, T., Canizares, C. R., et al. 2003, A&A, 402, 849
Packham, C., Young, S., Hough, J. H., et al. 1997, MNRAS, 288, 375
Pickles, A. J. 1998, PASP, 110, 863
Pier, E. A., & Krolik, J. H. 1993, ApJ, 418, 613
Rigaut, F., Salmon, D., Arsenault, R., et al. 1998, PASP, 110, 152
Rouan, D., Rigaut, F., Alloin, D., et al. 1998, A&A, 339, 687
Schinnerer, E., Eckart, A., Tacconi, L. J., et al. 2000, ApJ, 533, 850
Sosa-Brito, R. M., Tacconi-Garman, L. E., & Lehnert, M. D. 2001, ApJS, 136, 61
Tamura, M., Kleinman, S. G., Scoville, N. R., & Joyce, R. R. 1991, ApJ, 371, 131
Terlevich, R., Melnick, J., & Moles, M. 1987, IAUS, 121, 499
Terlevich, G., Tenario-Tagle, M., Rozyczka, et al. 1995, MNRAS, 272, 198
Thatte, N., Quirrenbach, A., Genzel, R., et al. 1997, ApJ, 490, 238
Thompson, R. I. 1996, ApJ, 459, L61
Thompson, R. I., Chary, R., Corbin, M. R., & Epps, H. 2001, ApJ, 558, L97
Unger, S. W., Lewis, J. R., Padlor, A., & Axon, D. J. 1992, MNRAS, 258, 371